Supporting information for

Polysulfide-Driven Low Charge Overpotential for Aprotic Lithium-Oxygen Batteries

Yin Zhou [a, b, c], Zhiyang Lyu [b], Zhenjie Liu [d], Wenrui Dai [b,c], Rui Guo [b], Jinlin Yang [b,c], Xinhang Cui [c, e], Yong Zhao[f], Ming Lin [g], Min Lai[a], Zhangquan Peng[d] and Wei Chen[b, c, e]*

[1]School of Physics and Optoelectronic Engineering, Nanjing University of Information Science & Technology, Nanjing 210044, Jiangsu, China

[2]Department of Chemistry, National University of Singapore, 3 Science Drive 3, 117543, Singapore.

[3]National University of Singapore (Suzhou) Research Institute, Suzhou, 215123, China.

[4]State Key Laboratory of Electroanalytical Chemistry, Changchun Institute of Applied Chemistry, Chinese Academy of Sciences, Changchun, Jilin, 130022, China

[5]Department of Physics, National University of Singapore, 2 Science Drive 3, 117543, Singapore.

[6] Institute for Advanced Study and Department of Physics, Nanchang University, Nanchang, 330031, P.R. China

[7]Institute of Materials Research and Engineering, A*STAR (Agency for Science, Technology and Research), 2 Fusionopolis Way. Innovis, Singapore.

*Corresponding Author E-mail: phycw@nus.edu.sg (W Chen)

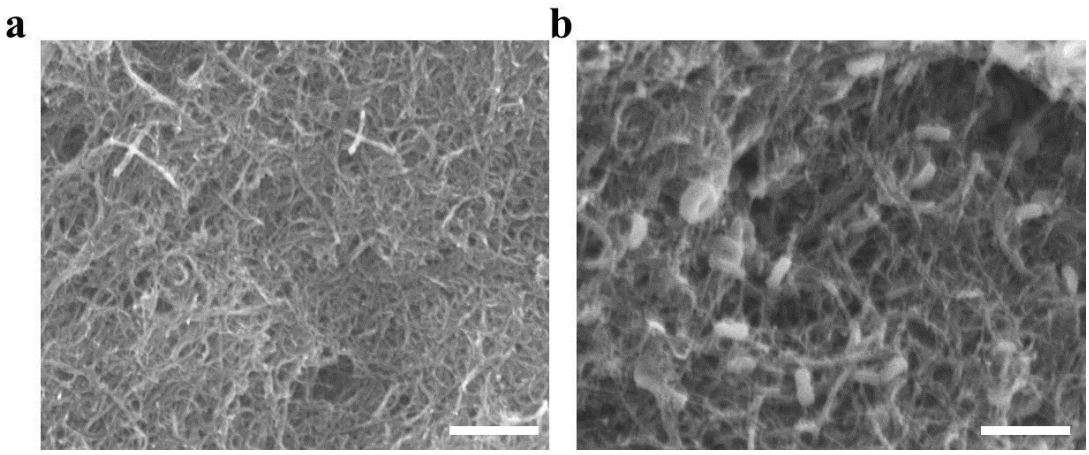

Figure S1. SEM images showing the morphology of CNT cathode (a) before charge and (b) after the 1st discharge. Scale bars, 200 nm (a), 500 nm (b).

Noted: The toroid-type products are observed after the 1st discharge process for CNT cathode.

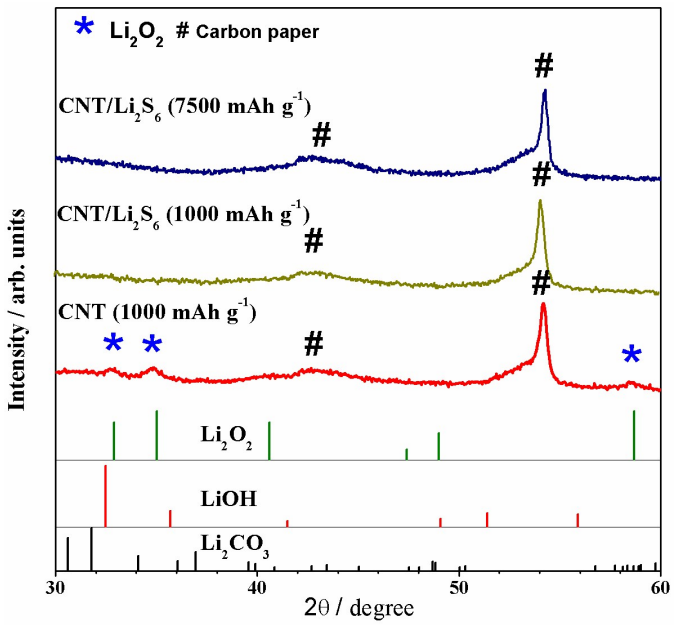

Figure S2. XRD patterns of CNT(1000 mAh g^{-1}) and CNT/Li_2S_6 (1000 mAh g^{-1} and 7500 mAh g^{-1}) after the 1st discharge.

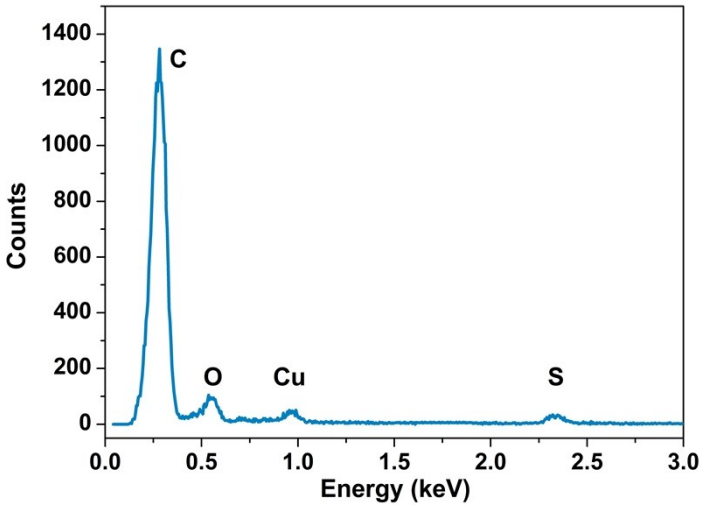

Figure S3. EDX result of the CNT/Li_2S_6 after the 1st discharge.

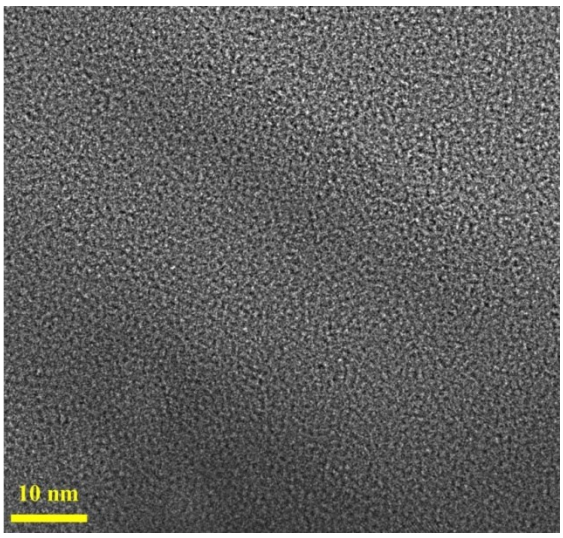

Figure S4. HR-TEM image for the 1st discharge products of CNT/Li_2S_6 cathode.

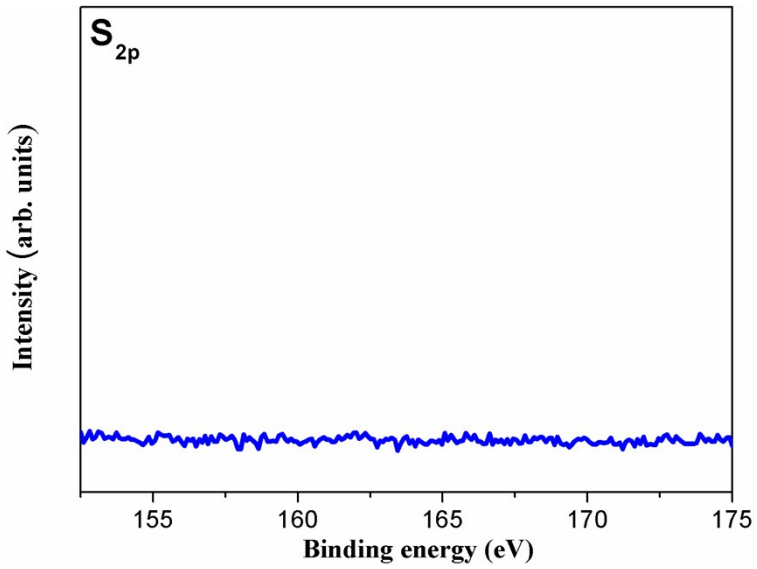

Figure S5. S 2p core-level XPS peak of the CNT cathode with Li_2S_6 additives before charge.

CNT was impregnated in the TEGDME solvent with Li_2S_6 additives, and then CNT was washed by acetonitrile and dried to do the XPS characterizations. We didn't observe any obvious S 2p in XPS, demonstrating that the Li_2S_6 additives can be fully washed away by acetonitrile. Therefore, after the 1st discharge, the S signal observed on the CNT/Li_2S_6 cathode mainly originates from the discharge product, not from the remained Li_2S_6 additives.

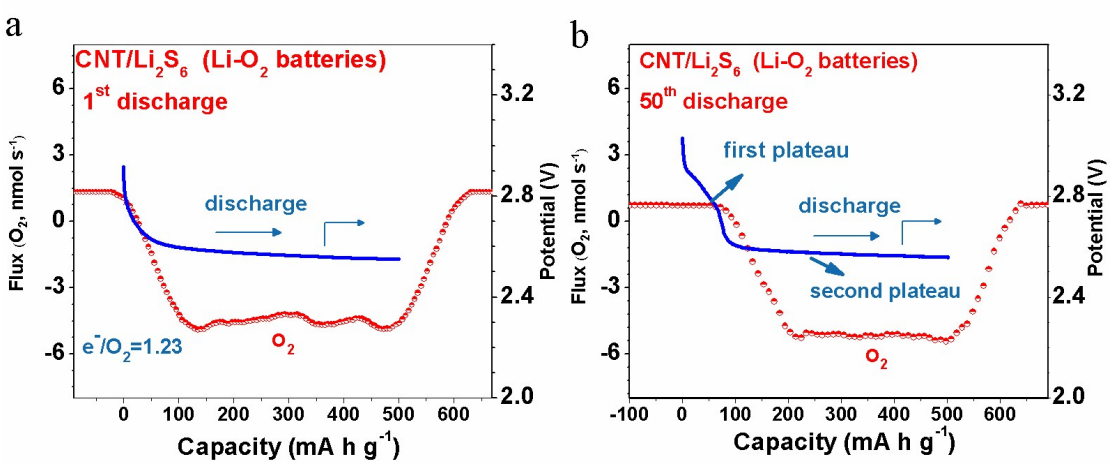

Figure S6. DEMS of CNT/Li_2S_6 for (a) the 1st and (b) the 50th discharge process at current of 0.7 mA at a limited capacity of 500 mAh g^{-1}.

The consumed ratio of electron and O_2 was confirmed by DEMS. O_2 is the only consumed gas and no evidence for the consumption of other gases (CO_2, H_2 etc.) during discharge process. The number of electrons per O_2 molecule for CNT/Li_2S_6 cathode is 1.23 (Figure S7a, Table S1). In addition, after the 50th discharge process, no O_2 consumption can be observed for the first platform.

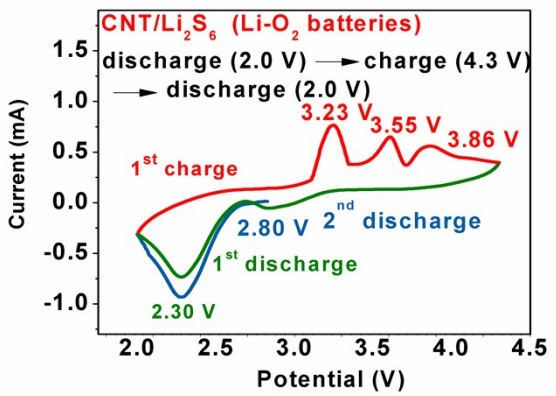

Figure S7. Cyclic voltammograms of CNT/Li_2S_6 under O_2, where CNT/Li_2S_6 is first discharged to 2.0 V, then charged to 4.3 V, and finally the CNT/Li_2S_6 cathode conducts the second discharge process to 2.0 V.

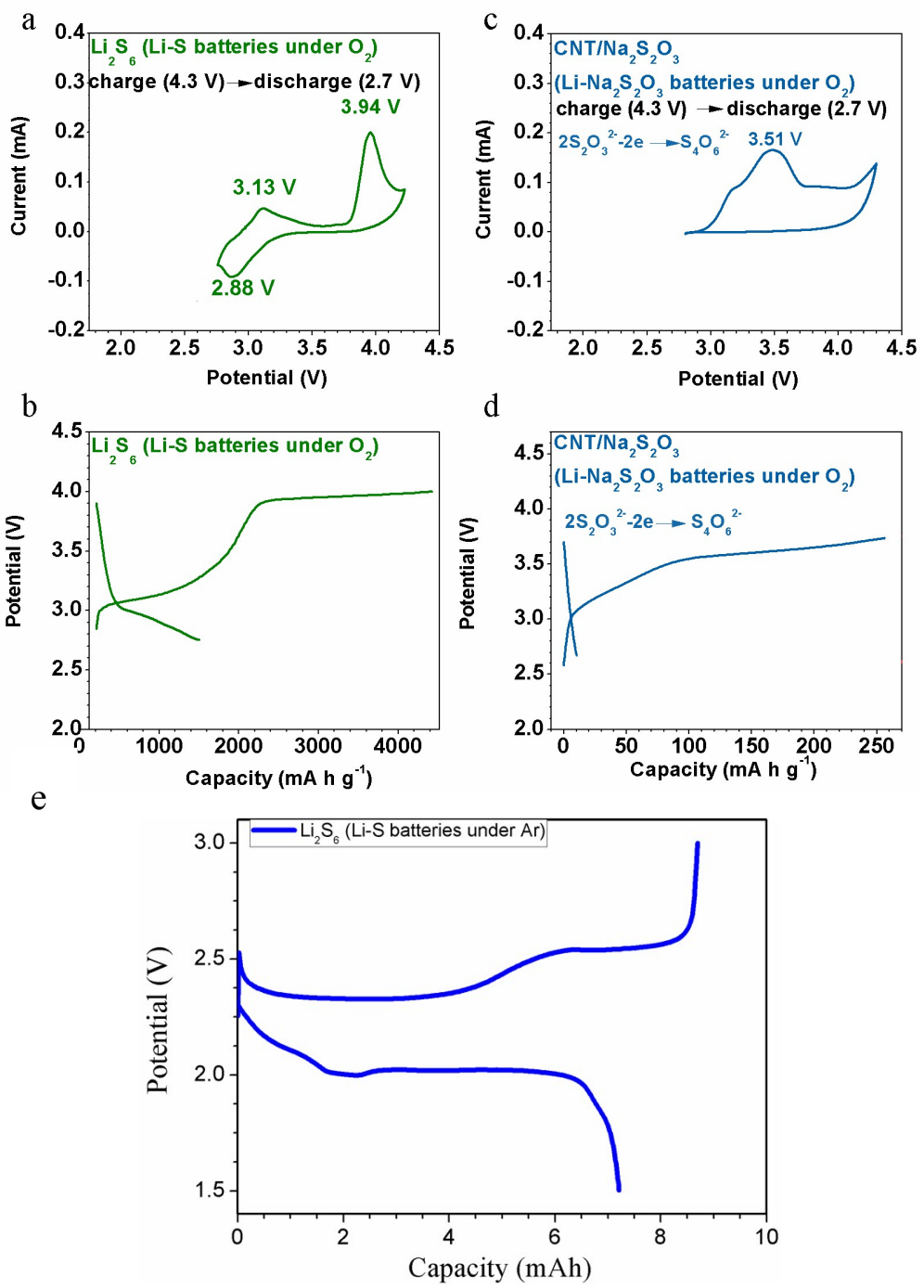

Figure S8. (a) Cyclic voltammograms and (b) the corresponding 1st charge-discharge curves (b) of Li_2S_6 (Li-S batteries under O_2), where Li_2S_6 is first charged to 4.3 V, and then is discharged to 2.7 V; (c) cyclic voltammograms and (d) the corresponding 1st charge-discharge curve of $Na_2S_2O_3$ (Li-$Na_2S_2O_3$ batteries under O_2), where $Na_2S_2O_3$ is first charged to 4.3 V, and then is discharged to 2.7 V, (e) discharge-charge curves of

the Li_2S_6 under Ar (Li-S batteries under Ar), where Li_2S_6 is first discharged to 1.5 V, and then is charged to 3.0 V.

Since $Li_2S_4O_6$ is inactive in TEGDME solvent,[1] polysulfide (Li_2S_2 and soluble Li_2S_6) and thiosulfate ($Li_2S_2O_3$) are main active materials for charge process. Therefore, the charge processes of polysulfide (Li_2S_2 and Li_2S_6) and $Li_2S_2O_3$ are separately studied by assembling two kinds of batteries: Li-S batteries (active materials: Li_2S_6 and Li_2S_2) and Li/$Na_2S_2O_3$ batteries (active materials: $Na_2S_2O_3$). Because the ORR occurred at 2.7 V, we should limit the discharge voltage of Li-S batteries and Li/$Na_2S_2O_3$ batteries above 2.7 V to separately study the discharge behavior. Therefore, we first charge the Li/$Na_2S_2O_3$ batteries and Li-S batteries to 4.0 V followed by discharging to 2.7 V under O_2 atmosphere.

For Li-S batteries, charge processes of Li_2S_2 and Li_2S_6 were separately conducted. In terms of charge process of Li_2S_6 (Li-S batteries under O_2), two typical peaks at 3.14 V and 3.94 V (Figure S8a) as well as corresponding charge curve (Figure S8b) are observed. The peak at 3.14 V corresponds to the oxidation of Li_2S_6 to high-order polysulfide (Li_2S_x, $6\leq x\leq 8$), while the peak at 3.94 V is ascribed to the oxidation of high-order polysulfide to sulfur (Figure S8a).[2] These two oxidation peaks are also be identified from CNT/Li_2S_6 cathode, implying that the peaks at 3.22 V and 3.86 V of CNT/Li_2S_6 are due to oxidation of low-order polysulfide (Li_2S_2 and Li_2S_6) to high-order polysulfide (equation 3, Li_2S_x, $6\leq x\leq 8$), and high-order polysulfide to sulfur, respectively.

For the oxidation process of $Na_2S_2O_3$ (Li-$Na_2S_2O_3$ batteries), the peak at 3.51 V (Figure S8c and S8d) is due to the oxidation of $Li_2S_2O_3$ to $Li_2S_4O_6$,[3] and the capacity of 258 mAh g^{-1} is near the theoretical capacity of $Na_2S_2O_3$ (339 mAh g^{-1}). Meanwhile, similar peak (3.55 V) is detected by charge process of CNT/Li_2S_6 cathode (Figure 3a), indicating that the middle peak of CNT/Li_2S_6 is due to the oxidation of $Li_2S_2O_3$ to $Li_2S_4O_6$.

For discharge process of Li-S batteries (active materials: Li_2S_6) under O_2, the peak at 2.84 V is due to the reduction of sulfur to high-order polysulfide (Li_2S_x, $6\leq x\leq 8$). In addition, inactive $Li_2S_4O_6$ is inactive and cannot be reduced from 4.0 V o 2.7 V.[3] Therefore, the new reduction peak at 2.84 V of CNT/Li_2S_6 belongs to the conversion of sulfur to high-order polysulfide (Li_2S_x, $6\leq x\leq 8$).

It should be noted that the voltage of oxidation and reduction plateaus of Li_2S_6 (Li-S batteries under O_2) under O_2 are different from the typical oxidation and reduction potential of lithium-sulfur (Li-S) batteries under Ar (Figure S8e). This is due to the fact that Li_2S_6 (Li-S batteries under O_2) is charged under O_2 atmosphere, resulting in the obviously positive voltage shift of both oxidation and reduction plateau.

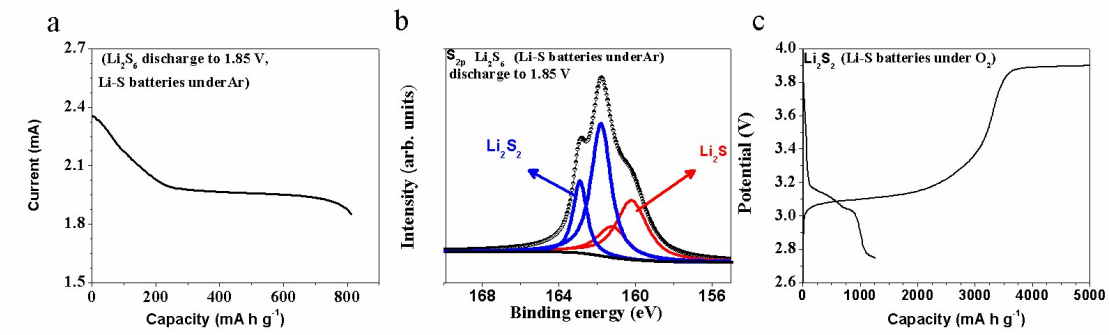

Figure S9. (a) Discharge curves of Li_2S_6 (Li-S batteries under Ar) when discharging to 1.85 V; (b) S 2p core level XPS spectrum of the discharge product when Li_2S_6 (Li-S batteries under Ar) is discharged to 1.85 V; (c) charge-discharge curves of Li_2S_2 (Li-S batteries under O_2). Li_2S_2 is first charged to 4.0 V, and then is discharged to 2.7 V.

Note: The mass of active materials in Figure S9a and Figure S9c is calculated by the mass of Li_2S_6, and CNT respectively.

For the oxidation process of Li_2S_2 under O_2, we obtained the Li_2S_2 when Li_2S_6 is discharged to 1.85 V under Ar. The main discharge product is Li_2S_2 despite the existence of Li_2S (Li-S batteries under Ar, Figure S9b). The Li_2S_2 is charged to 4.0 V, and then is discharged to 2.7 V under O_2 (Li-S batteries under O_2). During charge process, the platform at 3.14 V is due to the oxidation of Li_2S_2 to high-order polysulfide (Figure 9c, Li_2S_x, $6 \leq x \leq 8$), while the platform at 3.89 V is due to the oxidation of high-order polysulfide (Figure 9c, Li_2S_x, $6 \leq x \leq 8$) to sulfur. For discharge process, the discharge process from 3.2 V to 2.7 V is due to the reduction of sulfur to high-order polysulfide (Figure 9c, Li_2S_x, $6 \leq x \leq 8$)

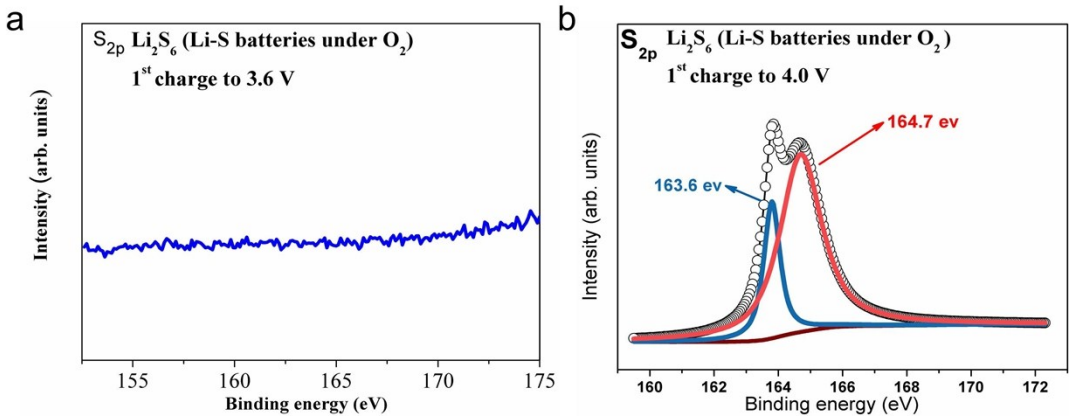

Figure S10. The Li_2S_6 additives were charged to 3.6 V and 4.0 V under O_2, respectively. (a) S 2p core level XPS spectrum of the discharge product when Li_2S_6 (under O_2) is charged to 3.6 V; (b) S 2p core level XPS spectrum of the discharge products when Li_2S_6 (under O_2) is charged to 4.0 V.

We separately charged the Li_2S_6 (Li-S batteries under O_2) to 3.6 V and 4.0 V. No S signal can be identified in XPS results when Li_2S_6 is charged to 3.6 V, indicating the charge process of Li_2S_6 from 3.0 V to 3.6 V is due to oxidation of Li_2S_6 to soluble high-order polysulfide (Li_2S_x, $6 \leq x \leq 8$). Due to high solubility of high-order polysulfide, high-order polysulfide is totally washed by acetonitrile and cannot be detected by XPS (Figure S10a). When Li_2S_6 is charged to 4.0 V (Li-S batteries under O_2), the typical S_{2p} peaks of charged products are in consistence with S_8 molecules. This result indicated that charge process of Li_2S_6 from 3.6 V to 4.0 V was due to oxidation of high-order polysulfide (Li_2S_x, $6 \leq x \leq 8$) to sulfur.

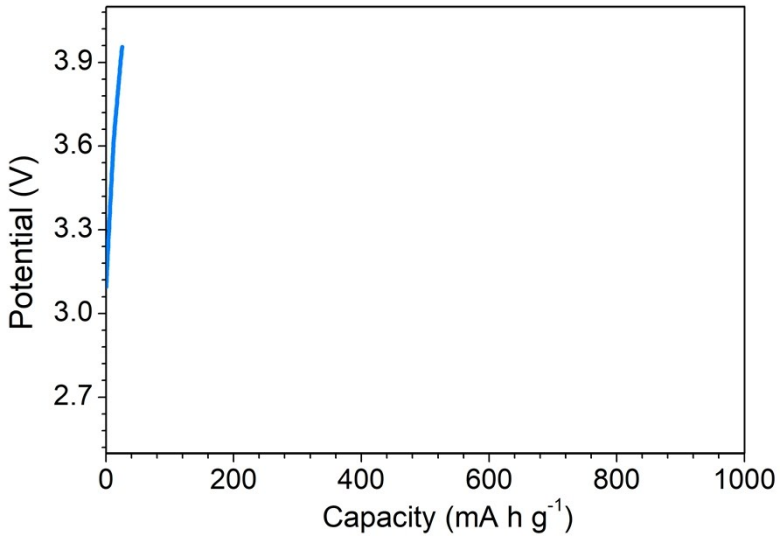

Figure S11. Charge profile of the CNT/S cathode under O_2.

The CNT/S cathode was charged from 3.0 V to 4.0 V under O_2. The voltage increases sharply and no obvious platform can be observed, indicating that sulfur is stable and cannot be oxidized from 3.0 V-4.0 V under O_2 atmosphere.

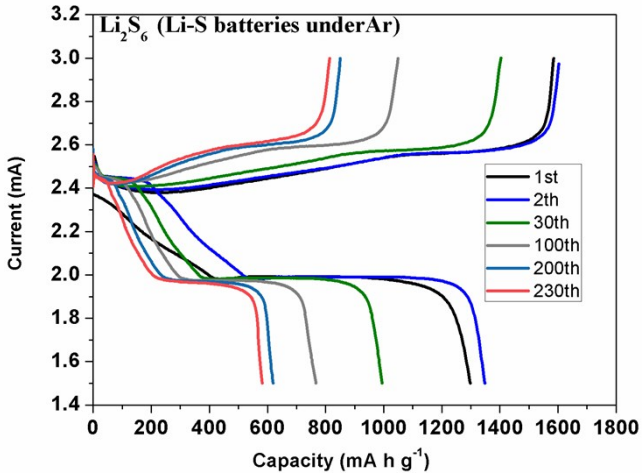

Figure S12. Cycle performance of Li_2S_6 (Li-S batteries under Ar). The higher charge capacity compared to the discharge capacity is due to the shuttle effect.

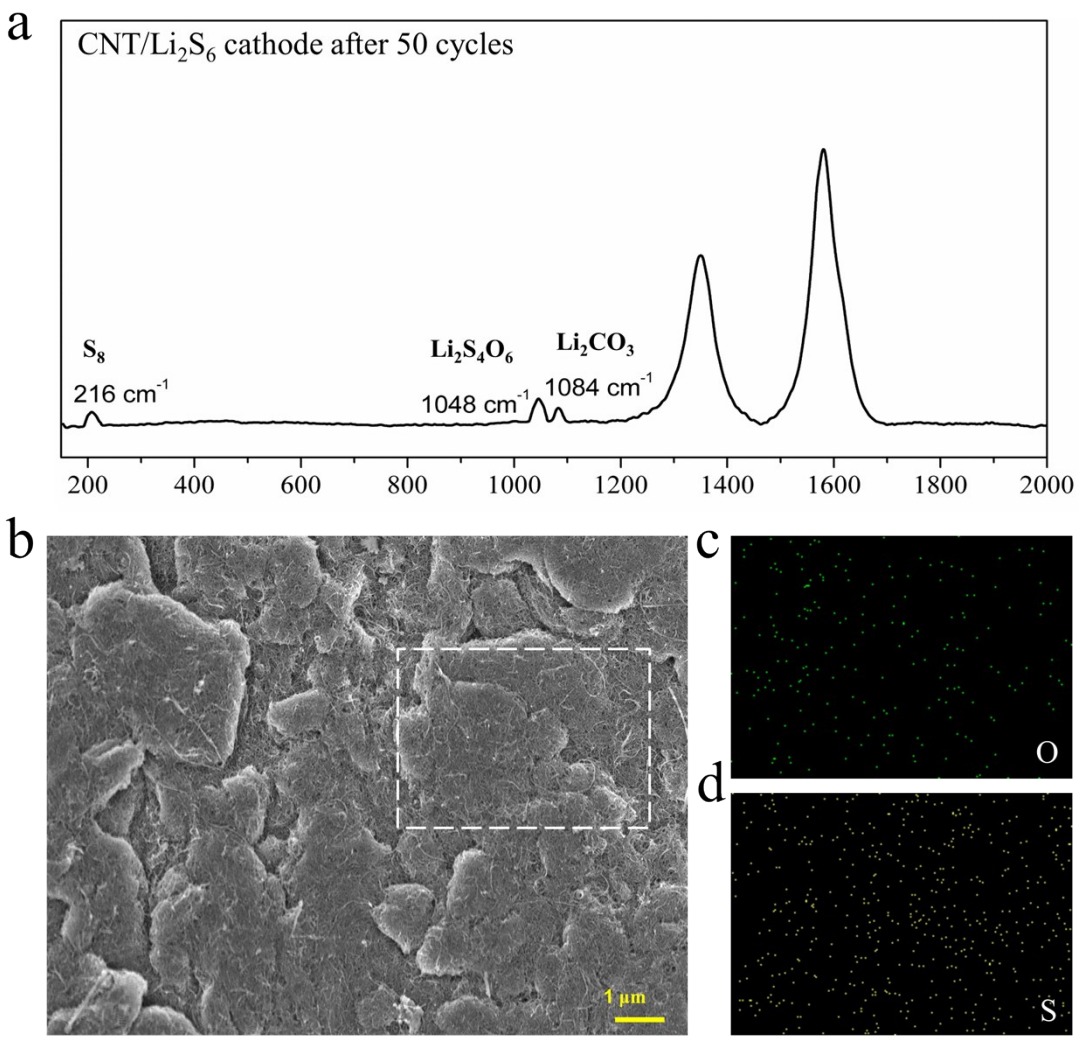

Figure S13. (a) Raman spectra of CNT/Li_2S_6 cathode after 50 cycles; (b) SEM images of CNT/Li_2S_6 cathode after 50th recharge; (c)-(d) EDX mapping of O and S for selected area in panel (b).

Table S1. O_2 electrochemistry quantified by DEMS: ratios of the number of electrons to oxygen molecules upon reduction (discharge process).

	Cycle number	discharge(e^-/O_2)
CNT(Li_2S_6)	1	1.23
	50	1.13

Table S2. Summary of carbon-based catalysts and their related performance.

Catalyst	Charge overpotential	Cycle performance	Ref
Au@cracked carbon submicron tube	1.3 V at 400 mA g^{-1}	112 cycles at 400 mA g^{-1} with 1000 mAh g^{-1}	[4]
Reduced graphene oxide (LiI)	around 0 V at 100 mA g^{-1}	2000 cycles at 1000 mA g^{-1} with 1000 mAh g^{-1}	[5]
Carbonized and activated wood/Ru	0.72 V at 0.1 mA cm^{-1}	100 cycles at 0.1 mA cm^{-1} with 0.6 mAh cm^{-1}	[6]
Mesoporous Carbon Nanocube/Ru ($LiNO_3$)	0.14 V at 200 mA g^{-1}	120 cycles at 400 mA g^{-1} with 1000 mAh g^{-1}	[7]
Polyethylene film@CNT	0.4 V at 2000 mA g^{-1}	610 cycles at 400 mA g^{-1} with 1000 mAh g^{-1}	[8]
Ketjen Black (UH_2O_2)	0.26 V at 100 mA g^{-1}	50 cycles at 500 mA g^{-1} with 1000 mAh g^{-1}	[9]
Textile	0.75 V at 0.1 mA cm^{-1}	50 cycles at 0.1 mA cm^{-1} with 1.0 mAh cm^{-1}	[10]
ZnO/VACNTs	0.63 V at 0.1 mA cm^{-1}	112 cycles at 0.1 mA cm^{-1} with 1000 mAh g^{-1}	[11]
CNT/Li_2S_6	**0.19 V at 0.5 A g^{-1}**	**147 cycles at 0.5 A g^{-1} with 500 mAh g^{-1}**	This work

References

[1] G. K. Druschel, R. J. Hamers, J. F. Banfield, Geochim. Cosmochim. Acta 2003, 67, 4457.

[2] T. Chen, L. Ma, B. Cheng, R. Chen, Y. Hu, G. Zhu, Y. Wang, J. Liang, Z. Tie, J. Liu, Z. Jin, Nano Energy 2017, 38, 239.

[3] J. Feng, D. C. Johnson, S. N. Lowery, J. Electrochem. Soc. 1995, 142, 2618; A. Pedraza, I. Villegas, P. Freund, B. Chornik, J. Electroanal. Chem. 1988, 250, 443.

[4] F. Tu, J. Hu, J. Xie, G. Cao, S. Zhang, S. A. Yang, X. Zhao, H. Y. Yang, Advanced Functional Materials 2016, 26, 7725.

[5] T. Liu, M. Leskes, W. Yu, A. J. Moore, L. Zhou, P. M. Bayley, G. Kim, C. P. Grey, Science 2015, 350, 530.

[6] H. Song, S. Xu, Y. Li, J. Dai, A. Gong, M. Zhu, C. Zhu, C. Chen, Y. Chen, Y. Yao, B. Liu, J. Song, G. Pastel, L. Hu, Advanced Energy Materials 2017, 1701203.

[7] B. Sun, S. Chen, H. Liu, G. Wang, Advanced Functional Materials 2015, 25, 4436.

[8] L. Wang, J. Pan, Y. Zhang, X. Cheng, L. Liu, H. Peng, Adv Mater 2017.

[9] S. Wu, Y. Qiao, S. Yang, M. Ishida, P. He, H. Zhou, Nat. Commun. 2017, 8, 15607.

[10] S. Xu, Y. Yao, Y. Guo, X. Zeng, S. D. Lacey, H. Song, C. Chen, Y. Li, J. Dai, Y. Wang, Y. Chen, B. Liu, K. Fu, K. Amine, J. Lu, L. Hu, Adv Mater 2017.

[11] W. Fan, B. Wang, X. Guo, X. Kong, J. Liu, Nano Energy 2016, 27, 577.